J. Fluid Mech. (2011), *vol.* 674, *pp.* 389–407.
doi:10.1017/S0022112010006555

Hydrodynamic interactions for the measurement of thin film elastic properties

S. LEROY AND E. CHARLAIX†

Laboratoire PMCN, Université de Lyon, CNRS UMR 5586, F-69622 Villeurbanne, France

(Received 23 June 2010; revised 22 October 2010; accepted 21 December 2010;
first published online 17 March 2011)

We study the elasto-hydrodynamic (EHD) interaction of a sphere with a flat elastic surface in the prospect of measuring the elastic moduli of soft supported thin films, with non-contact dynamic surface forces or atomic force microscopy measurements. When the sphere is oscillated at a very small amplitude close to the surface, the linear force response undergoes a dynamic transition from a viscous-dominated behaviour at large distance to an elastic-dominated behaviour at short distance. In the limit of very thin or very thick supported layers, we show that the force response obeys simple scaling laws which allow to unambiguously determine the absolute elastic modulus of the layer. In the general case, we establish the very rich phase diagram of the EHD interaction and discuss its application for optimizing experimental parameters.

Key words: lubrication theory, MEMS/NEMS, thin films

1. Introduction

Soft elastic films such as supported layers of polymers, elastomers, soft biologic tissues or even living cells are ubiquitous in nature and used increasingly in technological applications as diffusion or anti-corrosion barriers, dielectric coatings, electronic packaging, biocompatible layers, etc. The mechanical properties of these submicrometre thin films are of utmost importance for their stability and effective utilization; however, they can differ significantly from the bulk material due to the proximity of a supporting substrate. Owing to the large structural sizes involved in soft or biological matter, proximal effects induced by the interaction and organization of macro-molecules or self-assembled structures close to the wall can extend on scales comparable to the thickness of thin layers. In polymer melts for instance, variations up to four orders of magnitude of the mechanical properties in the close vicinity of a solid wall have been reported (Long & Lequeux 2001).

Conventional mechanical testing is not adapted for thin film investigation. As both the size and the stiffness are reduced, elastic forces become weaker than surface forces, adhesion and friction (Shull 2002). Besides, contact with a solid probe creates a new probe/layer interface, with new adhesion forces and possible modification of the material mechanics at its vicinity. Contact mechanics methods based on the Johnson–Kendal–Roberts (JKR) theory of elastic contact (Johnson, Kendall & Roberts 1971) simultaneaously measure the force, indentation and contact area of a spherical probe with the sample from which the Young's modulus and the work of adhesion can be independently determined. This approach used in surface force apparatus (SFA) and

† Email address for correspondence: elisabeth.charlaix@univ-lyon1.fr

similar devices is however limited to film thicknesses larger than the radius of the contact area, generally several tens of micrometres (Tardivat, Hervet & Leger 2001; McGuiggan *et al.* 2007). The JKR theory was extended to the case of thin layers by finite element (Johnson *et al.* 1971; Sridhar & Johnson 2004) or semi-analytical methods (Perriot & Barthel 2004; Barthel & Perriot 2007). However, mechanically confined layers exhibit a stiff response and their indentation is blurred by the one of the substrates (Gacoin *et al.* 2006; Mary, Chateauminois & Fretigny 2006). This elastic pile-up was shown especially severe for incompressible or quasi-incompressible materials such as polymers (Barthel *et al.* 2006), precluding accurate measurements on films thinner than some micrometres (Barthel 2007). The small probes used in scanning microscopies reduce the confinement, but do not allow to unambiguously account for the adhesion forces (Shull 2002), and are challenged to give more than relative values (Aime *et al.* 2001; Johannsmann 2002).

Non-conventional mechanical testing such as the inflation of nanobubbles (O'Connell & McKenna 2005), atomic force microscopy (AFM) in friction mode or in oscillatory mode (Basire & Fretigny 1999; Dubourg *et al.* 2003; McGuiggan 2004), dewetting or holes growth on a liquid substrate (Bodiguel & Fretigny 2006), quartz micro-balance (Leopoldes & Jia 2009) and lateral loading of contacts (Gacoin *et al.* 2006) provides valuable information on the mechanics of thin films, although absolute determination of elastic moduli relies on parameters which are difficult to measure accurately such as interfacial tension, wetting parameter or contact areas. The wrinkling instabilities method of Stafford *et al.* (2004) provides absolute values of the Young's modulus of thin films, but requires supporting substrates orders of magnitude softer, which limits its use for soft materials.

We propose here a new method to investigate the elastic properties of supported thin films, without contact, using the elasto-hydrodynamic (EHD) force induced by a moving sphere separated from the sample by a thin liquid layer. The advantage of this method is that the thin film is stressed not through the direct contact with a solid probe but through the drainage of a viscous Newtonian fluid, so that the resulting force does not include any adhesive contribution. EHD flows between a sphere and a plane have been studied theoretically and experimentally in the context of sphere collision and rebound in viscous liquids (Davis, Serayssol & Hinch 1986; Barnocky & Davis 1988, 1989; Vinogradova & Feuillebois 2000). The hydrodynamic force has been shown to depend strongly on the elastic modulus of the bodies when they are separated by a thin liquid layer. Here, we consider an harmonic EHD flow induced by a rigid sphere oscillating with a very small amplitude, and we study the resulting hydrodynamic force acting on a nearby elastic plane in the linear response limit. This type of mechanical testing can be implemented easily in SFA devices (Restagno *et al.* 2002) or AFMs. In this context, the oscillatory flow between a sphere and a plane covered with an array of bubbles has been studied theoretically by Lauga & Brenner (2004). They have discussed the reduction of the hydrodynamic force due to the surface compliance in terms of an apparent liquid slippage onto the solid. In this work, we establish the in-phase and out-of-phase components of the EHD force response in the general case of an elastic stratified surface. We show that these components undergo a transition from a viscous regime at large distance, towards an elastic regime at short distance. In the limit of very thin or very thick supported layers, the force response obeys simple scaling laws which allow to easily and unambiguously determine the absolute elastic modulus of the layer. In the general case, we establish the rich phase diagram of the EHD interaction and discuss its application for optimizing experimental parameters.

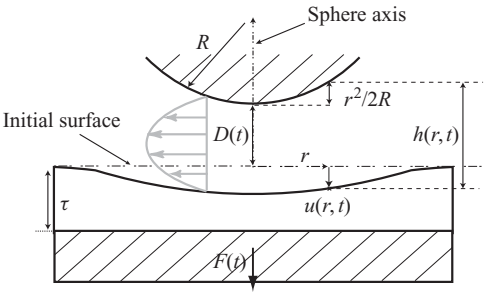

FIGURE 1. Principle of the method: a supported elastic layer is stressed through the drainage of a viscous liquid forced by the oscillatory motion of a spherical probe.

2. A linear response theory of EHD between a sphere and a plane

We consider the axisymmetric configuration sketched in figure 1 of an elastic film supported by a flat rigid substrate and immersed in a viscous liquid. A spherical probe at a nominal distance D of the plane oscillates in the normal direction with a nanometric amplitude $h_o \ll D$. The dynamic motion of the sphere creates an oscillating drainage flow and induces a pressure on the elastic surface. The quantity of interest is the hydrodynamic force response, i.e. the ratio of the complex amplitude F_ω of the dynamic force $F(t) = \mathrm{Re}[F_\omega \, \mathrm{e}^{i\omega t}]$ acting on the plane at the excitation frequency to the amplitude h_0 of the sphere oscillations $h_0 \cos(\omega t)$

$$G_\omega(D) = \frac{F_\omega}{h_0}. \tag{2.1}$$

Here, we focus on applications such as the SFA or the colloidal probe AFM, in which the distance $D(t) = D + h_0 \cos(\omega t)$ between the sphere apex and the plane is much lower than the probe radius R. The experimental frequency is at most in the range of kilohertz, the Reynolds number is very small (less than 10^{-2}) and the viscous penetration depth $\delta = \sqrt{\eta/\rho_f \omega} \ll D$ (with η as the liquid viscosity and ρ_f its density). In these limits, the drainage flow between the sphere and the plane is stable and laminar, and obeys the well-known lubrication equation (see Hocking 1973)

$$\frac{\partial}{\partial t}(h(r,t)) = \frac{1}{12\eta r}\frac{\partial}{\partial r}\left(r h(r,t)^3 \frac{\partial P(r,t)}{\partial r}\right), \tag{2.2}$$

with P as the liquid pressure. For this, the liquid chosen as a probe should retain its continuum character for all thicknesses $h(r,t)$ investigated. This is the case with simple liquids such as water, water solutions (sucrose, glycerol), alkanes and some other low molecular mass organic liquids down to thicknesses of 10 molecular size and less (Chan & Horn 1985; Georges *et al.* 1993; Raviv *et al.* 2004; Honig & Ducker 2007; Cottin-Bizonne *et al.* 2008). As we are interested only in the hydrodynamic interaction, the eventual effect of equilibrium long-range interaction forces such as van der Waals or electrostatic forces should be accounted for by subtracting their contribution to the measured force response, i.e. the derivative $\mathrm{d}F_{eq}(D)/\mathrm{d}D$ with $F_{eq}(D)$, the equilibrium force measured in a quasi-static experiment. Finally, we assume in (2.2) a no-slip boundary condition at the liquid–elastic layer interface. For this, the choice of a strongly non-wetting liquid should be avoided (Cottin-Bizonne *et al.* 2008; Huang *et al.* 2008). The absence of wall slippage can be checked self-consistently by looking at the viscous damping obtained at large distance, which does not depend on the elastic properties of the surface as shown later. However, the nanobubbles susceptible to

precipitate spontaneously at water/hydrophobic interfaces from dissolved gas (Yang *et al.* 2007; Ducker 2009) would provide an additional effective surface elasticity (see Lauga & Brenner 2004) not easily distinguishable from the intrinsic elastic response.

Equation (2.2) applied on a rigid plane gives a lubrication flow whose radial extension is of the order $\sqrt{2RD} \ll R$, called hereafter as the hydrodynamic probe radius. In the case of an *elastically* deformable plane, one has to take into account the displacement $u(r, t)$ of the surface at distance r of the axis (see figure 1). We restrict here to the quasi-static limit and do not consider the elastic wave generated by the oscillating stress: this is adequate for layers of shear moduli G in the order of kilopascals or more, for which the relevant frequency $\sqrt{G/2RD\rho_s}$ is much higher than the excitation frequency. We study the linear response obtained at a small forcing amplitude $h_o \ll D$, so that the film deflection $u(r, t)$ is also small compared to D. The liquid film thickness in the zone of interest is given by the parabolic approximation

$$h(r, t) = D + h_0 \cos\omega t + \frac{r^2}{2R} + u(r, t). \tag{2.3}$$

In the linear response regime, the time-dependent quantities are harmonic functions of time at the driving frequency. We write $u(r, t) = \mathrm{Re}[u(r)\,\mathrm{e}^{\mathrm{i}\omega t}]$ and $P(r, t) = P_0 + \mathrm{Re}[\delta P(r)\,\mathrm{e}^{i\omega t}]$, where P_0 is the ambient pressure, $u(r)$ and $\delta P(r)$ are complex amplitudes and we linearize (2.2) to the first order in h_0, u and δP

$$\mathrm{i}\omega r(h_0 + u(r)) = \frac{\partial}{\partial r}\left[\frac{r}{12\eta}\left(D + \frac{r^2}{2R}\right)^3 \frac{\partial \delta P(r)}{\partial r}\right]. \tag{2.4}$$

The small displacement approximation requires $h_0 + u(r, t) \ll D$. This is justified if $h_0 \ll D$ as the elastic deflection $u(r, t)$ can be at most equal to the sphere displacement. If one wishes to perform the experiment down to the lowest limit $D \simeq 5\,\mathrm{nm}$, where a simple liquid can safely be considered as a continuum, the amplitude of the sphere displacement h_0 has to be at most 1 Å, which is feasible in SFA devices.

The tangential stress σ_T at the surface is negligible compared to the normal stress: estimated in the case of a rigid surface, the ratio scales as $\sigma_T / P(r) \sim \sqrt{D/R} \ll 1$. Thus, one needs to only consider the coating response to the axisymmetric pressure acting on its surface. This response has been calculated independently by Li & Chou (1997) and by Nogi & Kato (1997), with a sticky boundary condition of the coating on the underlying substrate. The response relates the zeroth-order Hankel transforms of the normal displacement $u(r)$ to the one of the pressure $\delta P(r)$ (see Gacoin *et al.* 2006)

$$\tilde{u}(\xi) = \frac{2}{E^*}\frac{X(\xi\tau)}{\xi}\delta\tilde{P}(\xi), \tag{2.5}$$

where τ is the coating thickness, $E^* = E/(1 - \nu^2)$ its reduced Young's modulus, ν its Poisson ratio and $X(\xi\tau)$ the response function

$$X(\xi\tau) = \frac{\gamma(1 - \mathrm{e}^{-4\xi\tau}) - 4\xi\tau\,\mathrm{e}^{-2\xi\tau}}{\gamma(1 + \mathrm{e}^{-4\xi\tau}) + (\gamma^2 + 1 + 4(\xi\tau)^2)\,\mathrm{e}^{-2\xi\tau}}, \quad \gamma = 3 - 4\nu. \tag{2.6}$$

The zeroth-order Hankel transform and its inverse are obtained from the zeroth-order Bessel function of the first type J_o by

$$\tilde{u}(\xi) = \int_0^\infty r\,\mathrm{d}r\,J_0(\xi r)u(r), \quad u(r) = \int_0^\infty \xi\,\mathrm{d}\xi\,J_0(\xi r)\tilde{u}(\xi), \tag{2.7}$$

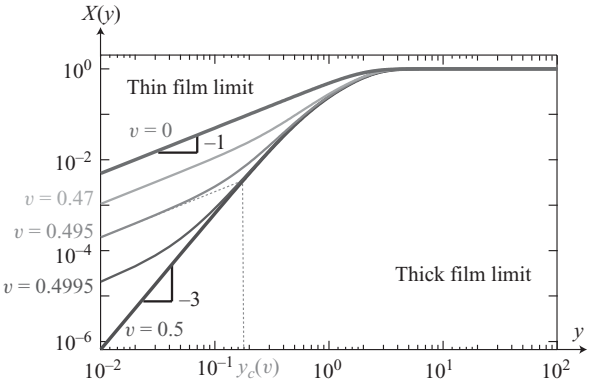

FIGURE 2. The variation of the film response (2.6) as a function of $y = \zeta\tau/\sqrt{2RD}$.

with a similar expression for $\delta\tilde{P}(\xi)$ (Abramowitz & Stegun 1964). A plot of $X(\xi\tau)$ as a function of $y = \xi\tau$ for various values of ν is shown in figure 2.

By integrating (2.4) between 0 and r, replacing $u(r)$ by its Hankel transform and using the relation $\int_0^r r'\,\mathrm{d}r' J_0(\xi r') = J_1(\xi r) r/\xi$, one gets the integro-differential equation

$$\frac{\partial \delta P(r)}{\partial r} = \frac{6\mathrm{i}\omega\eta h_0 r}{\left(D + r^2/2R\right)^3} + \frac{24\mathrm{i}De}{\left(D + r^2/2R\right)^3} \int_0^\infty \frac{X(\xi\tau)}{\xi} \delta\tilde{P}(\xi) J_1(\xi r)\,\mathrm{d}\xi, \tag{2.8}$$

where we have defined the Deborah number as $De = \eta\omega/E^*$. We introduce

$$x = \frac{r}{\sqrt{2RD}}, \quad \zeta = \xi\sqrt{2RD}, \quad \tau' = \frac{\tau}{\sqrt{2RD}}, \quad \delta P(r) = \frac{\eta\omega h_0 R}{D^2} p(x),$$
$$D_c = 8R\left(\frac{\eta\omega}{E^*}\right)^{2/3}, \tag{2.9}$$

so that $\delta\tilde{P}(\xi) = \tilde{p}(\zeta)(2\eta\omega h_0 R^2/D)$. Equation (2.8) takes the non-dimensional form

$$\frac{\partial p(x)}{\partial x} = 12\mathrm{i}\frac{x}{(1+x^2)^3} + \frac{3\mathrm{i}}{(1+x^2)^3}\left(\frac{D_c}{D}\right)^{3/2} \int_0^\infty \frac{X(\zeta\tau')}{\zeta} \tilde{p}(\zeta) J_1(\zeta x)\,\mathrm{d}\zeta. \tag{2.10}$$

Finally, a linear integral equation is obtained in the Hankel's space by performing the first-order transform of (2.10)

$$\left.\begin{aligned} \tilde{p}(\zeta) &= -\frac{3\mathrm{i}}{2}\zeta K_1(\zeta) - 3\mathrm{i}\left(\frac{D_c}{D}\right)^{3/2} \int_0^\infty \mathrm{d}\zeta' \tilde{p}(\zeta') X(\zeta'\tau') M(\zeta, \zeta'), \\ M(\zeta, \zeta') &= \int_0^\infty x\,\mathrm{d}x \frac{J_1(\zeta x) J_1(\zeta' x)}{\zeta'\zeta(1+x^2)^3}, \end{aligned}\right\} \tag{2.11}$$

with K_1 being the first-order modified Bessel function. The complex force response expressed as a function of $\tilde{p}(0)$ is

$$G_\omega(D) = -\frac{1}{h_0}\int_0^\infty 2\pi r\,\mathrm{d}r\,\delta P(r) = -\frac{4\pi\eta\omega R^2}{D}\tilde{p}(\zeta = 0). \tag{2.12}$$

Equations (2.11) and (2.12) together with the film response (2.6) determine completely the force response $G_\omega(D)$. In the case of a perfectly rigid film, the second term of the right member of (2.11) vanishes. As $K_1(\zeta) \sim 1/\zeta$ when $\zeta \to 0$, one recovers

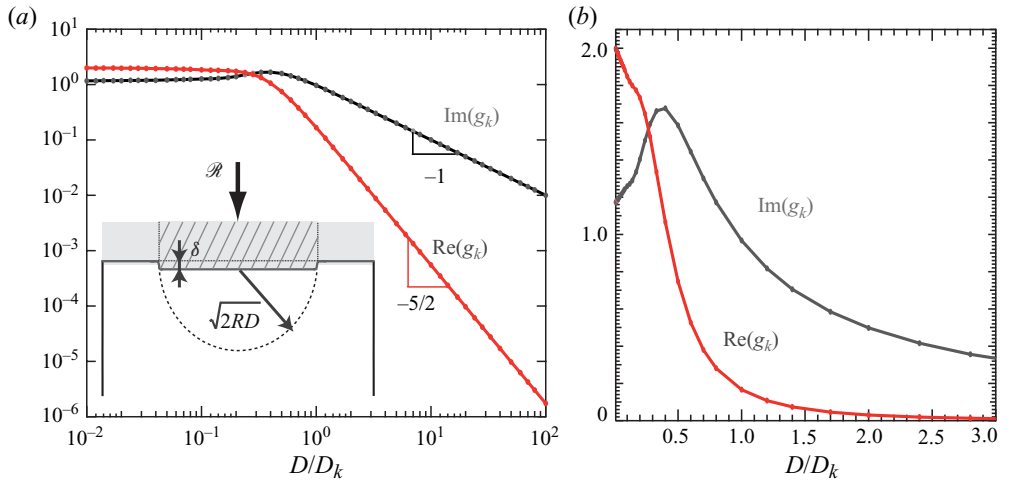

FIGURE 3. (Colour online) The components of the non-dimensional response function $g_k(D/D_k)$ defined in (3.3) as a function of D/D_k: (*a*) logarithmic scale, (*b*) linear scale. The inset represents a flat punch of radius $\sqrt{2RD}$ indenting a semi-infinite medium.

the expression of the hydrodynamic damping between a sphere and a rigid plane

$$G_\omega(D) = G'' = \mathrm{i}\,\frac{6\pi\eta\omega R^2}{D}. \tag{2.13}$$

3. The elastic and viscous regimes

A generic property of (2.11) and (2.12) is to yield two different rheological regimes for the variation of $G_\omega(D)$ as a function of D. These regimes are conveniently illustrated in the case of a semi-infinite elastic sample for which $X(y) = 1$. In this case, (2.11) reduces to

$$\tilde{p}(\zeta) = -\frac{3\mathrm{i}}{2}\zeta K_1(\zeta) - 3\mathrm{i}\left(\frac{D_k}{D}\right)^{3/2}\int_0^\infty \mathrm{d}\zeta'\tilde{p}(\zeta')\int_0^\infty x\,\mathrm{d}x\,\frac{J_1(\zeta x)J_1(\zeta' x)}{\zeta'\zeta(1+x^2)^3}, \tag{3.1}$$

$$D_k = D_c = 8R\left(\frac{\eta\omega}{E^*}\right)^{2/3}. \tag{3.2}$$

From (2.12), the force response function is given by the scaling law

$$G_\omega(D) = \frac{6\pi\eta R^2\omega}{D_k}\,g_k\left(\frac{D}{D_k}\right), \quad \text{where} \quad g_k\left(\frac{D}{D_k}\right) = -\frac{4D_k}{6D}\,\tilde{p}(\zeta = 0). \tag{3.3}$$

The function $g_k(D/D_k)$ is a non-dimensional complex function which is calculated numerically (see numerical procedure in Appendix A.2). The log–log scale plot of its real and imaginary part in figure 3 exhibits the two regimes, with a transition at $D = D_k$.

In the large distance regime $D \gg D_k$, the response is dominated by its imaginary part, the viscous damping, which is asymptotically equal to the Reynolds damping for rigid surfaces (2.13). In this viscous regime, the flow pressure is too low to significantly deform the surface. A rough estimate of the surface elastic indentation δ is obtained by taking the response of a semi-infinite elastic medium to a flat punch

of radius $\sqrt{2RD}$, applying uniformly the Reynolds force $\mathscr{R} = 6\pi\eta\omega h_0 R^2/D$. One gets $\delta \sim \mathscr{R}/E^*\pi\sqrt{2RD} = h_0(D_k/D)^{3/2}$. This estimate is similar to the result of Davis *et al.* (1986) in their study of the collision of two elastic spheres in a viscous fluid. They introduce the dimensionless elasticity parameter $\epsilon = \eta v_o R^{3/2}/E^* D^{5/2}$ and show that $\delta \sim D\epsilon$ when $\epsilon \ll 1$, which returns to our expression $v_o = h_0\omega$. Thus, the indentation remains small with respect to the amplitude of the sphere oscillations h_0 as long as $D > D_k$, which is precisely the limit of the viscous regime.

Pushing this estimation further, one can model the force response $G_\omega(D)$ by a spring-and-dashpot in series, by introducing the effective stiffness of the elastic layer $k(D) = \mathscr{R}/\delta \sim \pi E^*\sqrt{2RD}$, as well as the fluid friction coefficient associated to the Reynolds force $\lambda(D) = \mathscr{R}/h_0\omega$. This yields

$$G_\omega(D) \sim \left(\frac{1}{k} + \frac{1}{\mathrm{i}\omega\lambda}\right)^{-1} = \frac{\mathrm{i}k\omega\lambda}{k + \mathrm{i}\omega\lambda}. \tag{3.4}$$

In the viscous regime, $\omega\lambda/k = \delta/h_0 = (D_k/D)^{3/2} \ll 1$, so that

$$G_\omega(D) \sim \mathrm{i}\omega\lambda\left(1 - \mathrm{i}\frac{\delta}{h_0}\right) = \frac{6\omega\eta R^2}{D}(\mathrm{i} + (D_k/D)^{3/2}). \tag{3.5}$$

One retrieves, up to a numerical prefactor, the $D^{-5/2}$ power law of the elastic component displayed in figure 3 (see also Appendix A.1 for an analytical derivation).

When D becomes smaller than D_k, the components of the force response saturate to a constant value and have a similar magnitude. This is due to the fact that the indentation of the elastic surface cannot exceed the amplitude of the sphere oscillations. Therefore, the pressure in the liquid film saturates to the value $P_o \sim E^* h_0/\sqrt{2RD_k}$ for which this level of indentation is reached. The drainage flow between the sphere and the surface is now separated into two regions. At a distance lower than $\sqrt{2R(D_k - D)}$ of the sphere–plane axis, the indentation of the elastic surface compensates almost completely the sphere motion, and the liquid film clamped by its viscosity merely transmits the motion of the sphere. This provides the elastic component of the response $G' \sim P_o 2\pi R D_k/h_0 \sim E^*\sqrt{2RD_k}$. Outside this region, the pressure and the indentation decrease, and the features of the Reynolds flow are recovered. This provides the imaginary component of the response $G'' \sim 6\pi\eta\omega R^2/D_k \sim G'$.

Finally, the full force response of the semi-infinite elastic plane can be written as

$$\left.\begin{aligned} G_\omega(D) &= \frac{6\pi\eta R^2\omega}{D_k} g_k\left(\frac{D}{D_k}\right), \quad D_k = 8R\left(\frac{\eta\omega}{E^*}\right)^{2/3}, \\ \lim_{x\to 0} g_k(x) &= 2.015 + 1.163\mathrm{i} = 1.163(\sqrt{3} + \mathrm{i}), \\ \lim_{x\to\infty} g_k(x) &= \frac{3a_2}{16x^{5/2}} + \frac{\mathrm{i}}{x}, \quad a_2 = \int_0^\infty \zeta^2 K_1^2(\zeta)\,\mathrm{d}\zeta = \frac{3\pi^2}{32}, \end{aligned}\right\} \tag{3.6}$$

(see Appendix A.1 for the prefactors). Thus, the oscillatory EHD force response allows in principle to measure the elastic modulus E^* of a surface at a distance and without any contact through the value of $D_k = 8R(\eta\omega/E^*)^{2/3}$, from which E^* is derived. This is of interest for fragile surfaces which could be damaged or altered by a direct contact with a solid probe. We investigate in the next paragraph the case of thin films which is of wider interest for applications.

4. The case of a thin elastic coating

We now come back to (2.11) to discuss the behaviour of thin films. As the kernel $M(\zeta,\zeta')$ decays quickly when $\zeta'\to\infty$, as well as the pressure $\tilde{p}(\zeta')$, the significant domain of variation of the elastic response $X(\zeta'\tau')$ for a thickness $\tau\ll\sqrt{2RD}$ corresponds to $\zeta'\tau'\ll 1$. In this domain, $X(y)$ is essentially proportional to y (see figure 2) except close to the singular value $\nu=1/2$ of the Poisson ratio which corresponds to an incompressible material. Thus, we first investigate the two limit cases:

(i) compressible thin film $\nu<0.5$, $X(y)=y(1-2\nu)/(2(1-\nu)^2)$,
(ii) incompressible thin film $\nu=1/2$, $X(y)=(2/3)y^3$.

4.1. *The compressible thin film*

By injecting the simplified film response $X(y)=y(1-2\nu)/2(1-\nu)^2$ in (2.11), one gets the pressure equation for a compressible thin film

$$\tilde{p}(\zeta)=-\frac{3\mathrm{i}}{2}\zeta K_1(\zeta)-3\mathrm{i}\left(\frac{D_n}{D}\right)^2\int_0^\infty \zeta'\,\mathrm{d}\zeta'\,\tilde{p}(\zeta')M(\zeta,\zeta'), \tag{4.1}$$

$$D_n=\sqrt{\frac{8\eta\omega R\tau}{E'}},\quad E'=\frac{E(1-\nu)}{(1-2\nu)(1+\nu)}, \tag{4.2}$$

with the force response

$$\left.\begin{aligned} &G_\omega(D)=\frac{6\pi\eta R^2\omega}{D_n}g_n(D/D_n),\quad g_n(D/D_n)=-\frac{4D_n}{6D}\tilde{p}(0),\\ &\lim_{x\to 0}g_n(x)=1.633(1+\mathrm{i})=\sqrt{\frac{8}{3}}(1+\mathrm{i}),\\ &\lim_{x\to\infty}g_n(x)=\frac{3a_3}{16}\frac{1}{x^3}+\frac{\mathrm{i}}{x},\quad a_3=\int_0^\infty\zeta^3K_1^2(\zeta)\,\mathrm{d}\zeta=\frac{2}{3}. \end{aligned}\right\} \tag{4.3}$$

The force response (see figure 4) displays the viscous and the elastic regimes discussed in the previous section with a cross-over at $D=D_n$. But the cross-over distance now involves the square root of the film thickness and the elastic coefficient for uniaxial strain $E'=E(1-\nu)/(1-2\nu)(1+\nu)$. Another qualitative change is the D^{-3} decay of the real component in the viscous regime instead of $D^{-5/2}$ in the thick film case. These features are explained by considering the indentation δ of the film in the viscous regime. As the width $\sqrt{2RD}$ of the hydrodynamic probe is much larger than the film thickness, the response of the film is essentially local. It can be modelled as a uniform uniaxial strain in the z direction, as the portions of the film far from the sphere–plane axis are clamped by the sticking boundary condition on the substrate and prevent a significant expansion in the xy directions. Therefore, the indentation scales as $\delta/\tau\sim(\mathscr{R}/2\pi RD)/E'$ with $\mathscr{R}=6\pi\eta\omega h_o R^2/D$ being the Reynolds force. This gives $\delta/h_0\sim 3\eta\omega R\tau/E'D^2=(D_n/D)^2$. The indentation equals the sphere oscillations' amplitude at $D=D_n$. Furthermore, the effective stiffness of the elastic film is now $k(D)=\mathscr{R}/\delta=2\pi RDE'/\tau$. Therefore, the spring-and-dashpot model of the previous section (3.4) leads to the force response $G_\omega(D)\sim(6\pi\eta\omega R^2/D)(\mathrm{i}+(D_n/D)^2)$ in the viscous regime.

A few remarks are in order. Firstly, the response of a very thin film is essentially local, i.e. the amplitude of the film surface displacement is proportional to the amplitude of the local pressure: $u(r)=\tau P(r)/E'$. Thus, the EHD dynamic response can be calculated in the real space using (2.4) (see Appendix A.3). This approach has

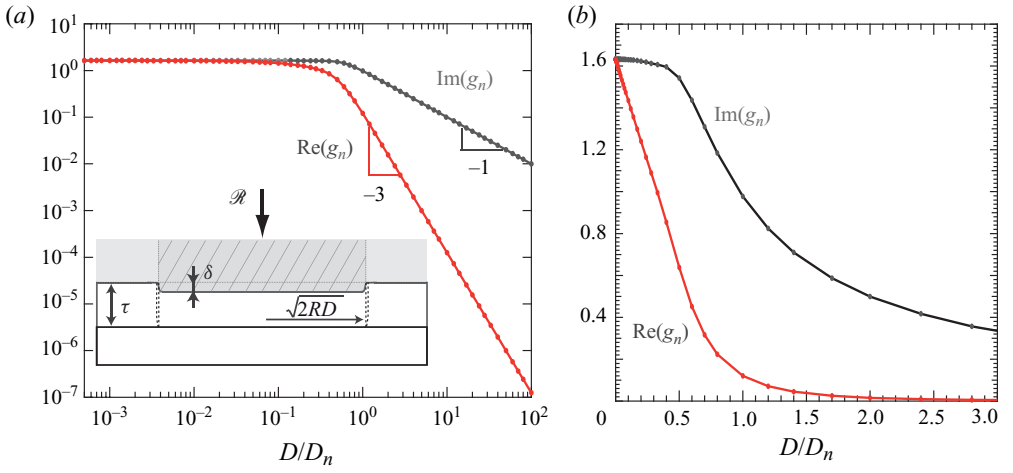

FIGURE 4. (Colour online) The components of the non-dimensional response function $g_n(D/D_n)$ defined in (4.3) as a function of D/D_n: (*a*) logarithmic scale, (*b*) linear scale. The inset represents a flat punch of radius $\sqrt{2RD}$ indenting a compressible layer of thickness τ.

been followed by Steinberger *et al.* (2008) to model dynamic surface force experiments on a superhydrophobic surface in the so-called Cassie wetting, i.e. with a network of micro-bubbles embedded at the solid–liquid interface. Indeed, a bubble mattress can be considered as a model case of an infinitely thin elastic film: the bubbles trapped at the interface are affected independently of each other by the flow, and their deformation depends only on the local pressure. Steinberger *et al.* (2008) introduce a local stiffness to account for the elastic linear response of the bubble mattress. Our force response $G_\omega(D)$ is exactly equivalent to theirs, taking the value E'/τ as the local stiffness in their theory. The excellent agreement of their experimental results with the EHD theory illustrates the power of the method to investigate soft and fragile surfaces which do not allow direct mechanical contact.

Secondly, as noted in the previous section, the force response of the compressible thin film depends only on the parameter D_n once other experimental values are determined; so it gives access only to the uniaxial modulus E' of the film. However, the notion of a very thin film is relative to the size of the hydrodynamic probe which depends on D. A way to determine the two moduli E and ν of a given film is then to investigate both thick and thin film limits by an adequate choice of probe radius and range of distance D. This point is further discussed in § 5.

4.2. *The incompressible thin film*

Injecting the film response $X(y) = 2y^3/3$ into the master equation (2.11) yields the pressure equation for the incompressible thin film

$$\tilde{p}(\zeta) = -\frac{3\mathrm{i}}{2}\zeta K_1(\zeta) - 3\mathrm{i}\left(\frac{D_{1/2}}{D}\right)^3 \int_0^\infty \zeta'^3 \,\mathrm{d}\zeta' \tilde{p}(\zeta') M(\zeta, \zeta'), \tag{4.4}$$

$$D_{1/2} = \tau\left(\frac{16\eta\omega}{3E^*}\right)^{1/3} = \tau\left(\frac{4\eta\omega}{3G}\right)^{1/3}, \tag{4.5}$$

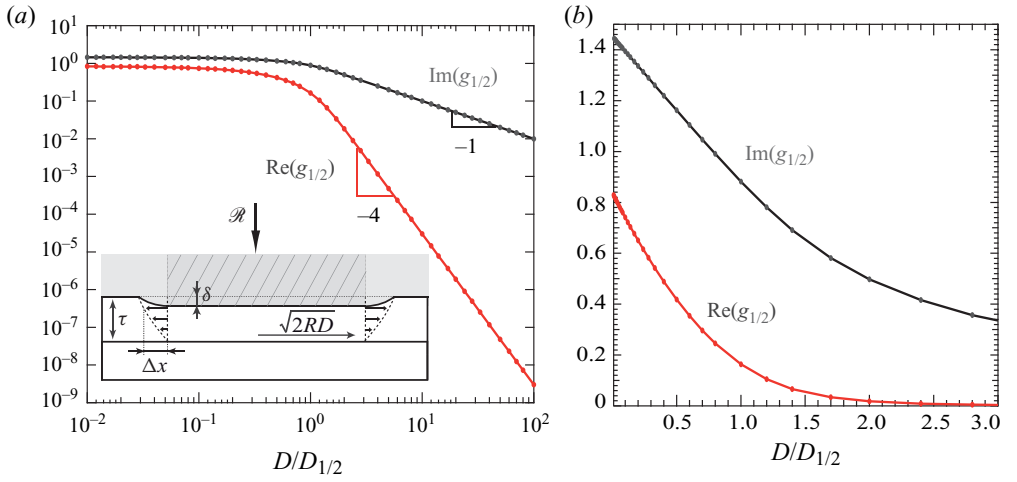

FIGURE 5. (Colour online) The components of the non-dimensional response function $g_{1/2}(D/D_{1/2})$ defined in (4.6) as a function of $D/D_{1/2}$: (*a*) logarithmic scale, (*b*) linear scale. The inset represents a flat punch of radius $\sqrt{2RD}$ indenting an incompressible layer of thickness τ.

which gives the force response and its asymptotic limits

$$G_\omega(D) = \frac{6\pi\eta R^2\omega}{D_{1/2}}\, g_{1/2}\left(\frac{D}{D_{1/2}}\right), \quad g_{1/2}\left(\frac{D}{D_{1/2}}\right) = -\frac{4D_{1/2}}{6D}\tilde{p}(\zeta=0), \tag{4.6}$$

$$\lim_{x\to 0} g_{1/2}(x) = 0.838(1+\mathrm{i}\sqrt{3}), \tag{4.7}$$

$$\lim_{x\to\infty} g_{1/2}(x) = \frac{3a_5}{16x^4} + \frac{\mathrm{i}}{x}, \quad a_5 = \int_0^\infty \zeta^5 K_1^2(\zeta)\,\mathrm{d}\zeta = 8/5. \tag{4.8}$$

The cross-over distance $D_{1/2}$ between the viscous and the elastic regimes now no longer depends on the sphere radius R but only on the length scale τ. This is a much smaller distance, as we are in the thin film limit $\tau \ll R$. Also, in the viscous regime, the real part of the force response decays as D^{-4} instead of D^{-3} in the compressible case (figure 5). Finally, the real component is always lower than the imaginary component, even in the elastic regime. These features underline a much stiffer behaviour of the incompressible thin film as compared to the compressible one, at an equivalent Young's modulus E^*.

This stiffer behaviour is due to the fact that as the volume of the thin layer is conserved, its indentation has to be compensated by a lateral displacement, which is no longer negligible although it is strongly hampered by the sticking boundary condition on the underlying substrate. Let Δx be the lateral displacement of the film surface at a distance x from the sphere–plane axis (see figure 5). Due to the volume conservation, $2\pi x\tau\,\Delta x = \pi x^2\delta$; thus, the shear strain of the film is $\Delta x/\tau = x\delta/2\tau^2$. In the viscous regime, the maximum shear deformation at the border of the stressed area $x = \sqrt{2RD}$ reaches $\epsilon_{max} = \sqrt{2RD}\,\delta/2\tau^2$. One can then estimate the indentation δ by equating the elastic energy stored in the sheared film, $E_{el} \sim (1/2)G\epsilon_{max}^2 2\pi RD\tau$ to the work provided by the Reynolds force $\mathscr{R}\delta$. This gives $\delta/h_0 = 12(\eta\omega/G)\tau^3/D^3$, which retrieves the value of the cross-over distance $D_{1/2}$ up to a numerical prefactor. The effective stiffness $k(D) = \pi R^2D^2G/2\tau^3$ of the incompressible thin film grows more quickly with the distance D than the other limit cases. The spring-and-dashpot

model (3.4) $G_\omega(D) = (6\pi\eta\omega R^2/D)(\mathrm{i} + \delta/h_0)$ retrieves also the D^{-4} decay of the elastic part of the force response in the viscous regime.

The severely stiff response of incompressible thin layers in the mechanics of solid contacts has been discussed in the context of the so-called 'JKR tests' for measuring the elastic properties of thin films (Barthel *et al.* 2006; Gacoin *et al.* 2006). In particular, Barthel (2007) has discussed in detail the interpretation of JKR tests performed by Tardivat *et al.* (2001), and shown that due to elastic pile-up, it is not possible in a JKR test to extract with a good accuracy the Young's modulus of a coating of thickness less than some micrometres if its Poisson ratio is 1/2. The difficulty in the JKR test stems from the fact that as hard contact is involved, the indentation on the sphere–plane axis is forced, and the stressed area depends on its amplitude. In the nanorheology method, the fluid probe spreads the stress over a wide area whereas the indentation is limited to the amplitude of the sphere oscillation.

The spring-and-dashpot model can also be used to estimate the impact of the substrate by comparing its effective stiffness $k_s(D) = E_s^* \pi \sqrt{2RD}$ (with E_s^* as the reduced modulus of the substrate) to the stiffness $k(D) = \pi R^2 D^2 G/2\tau^3$ of the incompressible layer. If necessary, the substrate can be included quantitatively in the EHD model via the full response of the layered system, calculated by Li & Chou (1997) (see Appendix A.4). The effect of substrate stiffness is less than 1 % if

$$\tau > 2.1 \left(\frac{E^*}{E_s^*}\right)^{1/3} \sqrt{RD}. \tag{4.9}$$

Thus, with an SFA of sphere radius $R = 3\,\mathrm{nm}$ used at a distance $D = 20\,\mathrm{nm}$, it is possible to investigate films of 200 nm with a Young's modulus in the range of 10 MPa deposited on a glass substrate. With an AFM of colloidal probe radius 10 μm, the same range of modulus would be accessible down to a thickness of some nanometres, without the need of measuring a contact area.

5. The general case: a dynamic phase diagram

The limit cases studied in the previous sections involve only one elastic parameter, combination of E and ν, and the force response in these cases is given by a master function depending only on a reduced variable D/D_c. This is convenient to fit experimental data and extract the corresponding elastic parameter of the layer. However in the general case, such a scaling is not possible anymore and the general solution of (2.11) has to be used. We establish here the phase diagram of this general solution in the $(D/R, \tau/R)$ plane, discuss the use of this phase diagram for optimizing experimental parameters and present the variation of the components of the force response in optimized experimental runs.

The general equation (2.11) shows three different transitions. Firstly, the transition between a thin and a thick layer is governed by the ratio of the thickness τ to the hydrodynamic radius $\sqrt{2RD}$. The transition is obtained for $\tau/R = \sqrt{2D/R}$ which is a line of slope 1/2 in the $(\log D/R, \log \tau/R)$ plane (see figure 6). The thick film region lies above this line and the thin film lies under.

The second transition is between the compressible and the incompressible thin film. The value $\nu = 1/2$ of the Poisson ratio is indeed singular and associated to a critical behaviour. When ν is close to 1/2, the film's response $X(y)$ in the range $y < 1$ (thin film) is dominated by the non-critical behaviour $y(1-2\nu)/2(1-\nu)^2$ at small y and

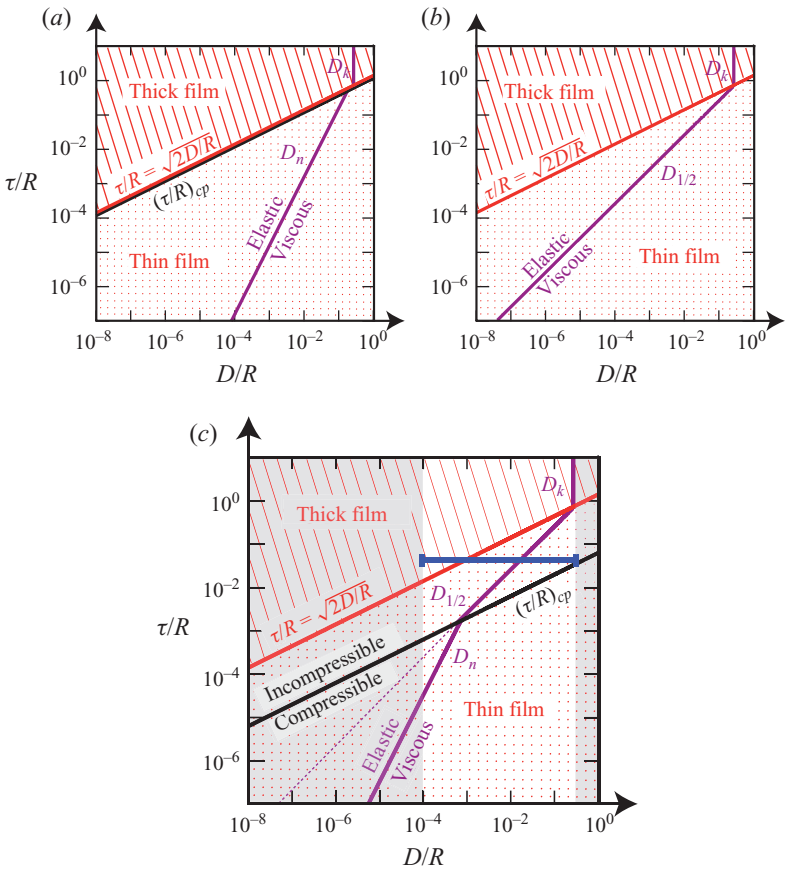

FIGURE 6. Dynamic phase diagram for the value (*a*) $\nu = 0$, (*b*) $\nu = 0.5$, and (*c*) $\nu = 0.499$. The continuous red line is the thick/thin transition, and the parallel black line in (*a*) and (*c*) is the compressible–incompressible transition. The incompressible thin film domain lies between those lines. The purple lines are the elastic/viscous cross-over distances D_k, D_n and $D_{1/2}$ in each domain (see their expression in table 1). In (*c*), the horizontal blue line is an example of experimental run which crosses several transitions.

reaches the critical behaviour $2y^3/3$ at $y_c(\nu) = \sqrt{3(1-2\nu)/4(1-\nu)^2}$ (see figure 2). Therefore, the compressible/incompressible transition at $\tau' = \tau/\sqrt{2RD} = y_c$ can be written as

$$\left(\frac{\tau}{R}\right)_{cp} = \sqrt{\frac{3(1-2\nu)}{2(1-\nu)^2}\frac{D}{R}} < \sqrt{\frac{2D}{R}}. \tag{5.1}$$

This transition is parallel to the thick/thin transition line. The incompressible region lies between the two lines. However, when $\nu \lesssim 0.45$, both transitions are very close to each other and the incompressible thin film behaviour is too shallow to be observed. When $\nu \to 1/2$, the incompressible transition line (5.1) shifts downwards to infinity and the incompressible behaviour progressively fills the whole thin film region.

Finally, the elastic and viscous regimes have to be located in each region. This is done by considering the cross-over distances D_k, D_n and $D_{1/2}$ which give the three

$\frac{G_\omega(D)}{6\pi\eta\omega R^2}$	Elastic regime	Viscous regime	Cross-over distance
Thick film	$\frac{1.163}{D_k}(\sqrt{3}+\mathrm{i})$	$\frac{9\pi^2}{512}\frac{D_k^{3/2}}{D^{5/2}}+\frac{\mathrm{i}}{D}$	$D_k = 8R\left(\frac{\eta\omega(1-\nu^2)}{E}\right)^{2/3}$
Compressible thin film	$\frac{1.633}{D_n}(1+\mathrm{i})$	$\frac{1}{8}\frac{D_n^2}{D^3}+\frac{\mathrm{i}}{D}$	$D_n = \sqrt{\frac{8\eta\omega R\tau(1-2\nu)(1+\nu)}{E(1-\nu)}}$
Incompressible thin film	$\frac{0.838}{D_{1/2}}(1+\mathrm{i}\sqrt{3})$	$\frac{3}{10}\frac{D_{1/2}^3}{D^4}+\frac{\mathrm{i}}{D}$	$D_{1/2} = \tau\left(\frac{16\eta\omega(1-\nu^2)}{3E}\right)^{1/3}$

TABLE 1. Summary of the limit behaviour of the force response in each region of the phase diagram.

equations

$$\frac{D_k}{R} = 8\left(\frac{\eta\omega}{E^*}\right)^{2/3}, \quad \left(\frac{\tau}{R}\right)_{1/2} = \left(\frac{3G}{4\eta\omega}\right)^{1/3}\frac{D_{1/2}}{R}, \quad \left(\frac{\tau}{R}\right)_n = \frac{E'}{8\eta\omega}\left(\frac{D_n}{R}\right)^2, \tag{5.2}$$

each valid in their domain. The elastic/viscous cross-over for the thick film does not depend on its thickness and is a vertical line in the $(D/R, \tau/R)$ plane. The incompressible elastic/viscous cross-over $(\tau/R)_{1/2}$ is a straight line of slope 1. Note that when $\nu \to 1/2$, this cross-over line does not change much as it depends on the shear modulus of the layer. But the two other lines, the elastic/viscous cross-over $(\tau/R)_n$ in the compressible thin film domain and the incompressible transition $(\tau/R)_{cp}$ are shifted downwards to infinity when $\nu \to 1/2$. The intercept of these two lines is located on the cross-over line $(\tau/R)_{1/2}$.

The phase diagrams for three different values of ν (0, 0.499 and 1/2) are plotted in figure 6, and the limit behaviour of the force response in each region is summarized in table 1. It must be emphasized that the transitions and the cross-overs are not sharp, so that the limit behaviours are fully obtained only in the heart of the corresponding regions, at half a decade or so from their limits.

The phase diagram can be used to optimize the experimental parameters. In SFA or AFM experiments, an experimental run is characterized by a horizontal line (see figure 6) whose lateral extension is the range of available distances allowed by the experimental set-up. Changing the probe radius translates this 'run-line' along the first diagonal of the diagram. If the Poisson ratio of the layer is known or expected to change very weakly with the thickness, the best choice of probe radius is when the run-line investigates the heart of a region at least a decade far from its border, so that a master function can be used for adjusting the data by a simple translation in the log–log scale. However, if one wishes to determine both the Young's modulus and the Poisson ratio of the film in one run, the run-line should cross different regions to take benefit of the different combinations of the elastic moduli governing each limit case. Then, the entire equation (2.11) has to be used to extract the moduli. The other experimental parameter, the liquid viscosity, defines the horizontal position of the cross-over lines D_k, $D_{1/2}$ and D_n in the phase diagram. The force response is most sensitive to the elastic behaviour of the layer in the elastic regime; however, if the probe radius is not accurately known , locating the elastic/viscous cross-over in the middle of the run-line allows the experimental determination of the product ηR^2 from the $1/D$ decay of the damping in the viscous regime.

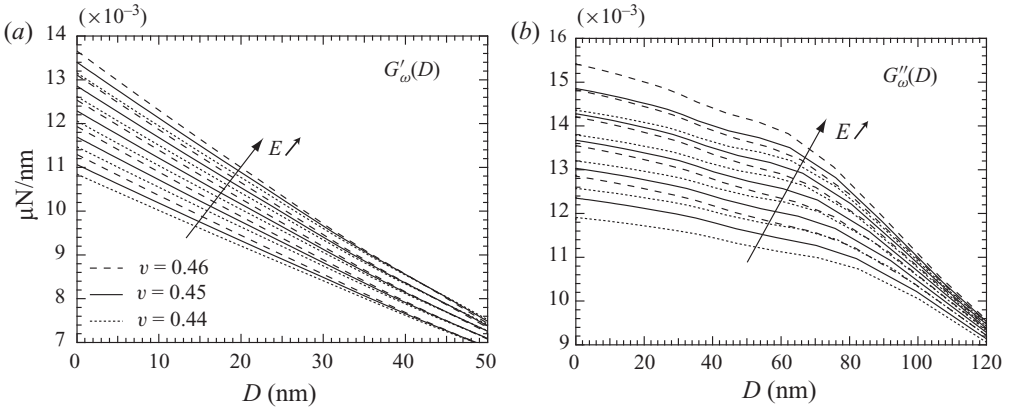

FIGURE 7. Illustration of the determination of the Young's modulus and the Poisson ratio of a 1 μm thick polymer film ($\nu > 0.4$) probed with a colloidal probe AFM of radius $R = 10\,\mu$m at a frequency $f = 1$ kHz and with a fluid of viscosity $\eta = 100$ mPa s. A first estimation of the Young's modulus using the function g_n (4.3) gives the magnitude $E = 1$ MPa and $\nu = 0.45$. The solutions of the full equation (2.11), (2.12) are plotted for $E = 0.8$, 0.9, 1, 1.1 and 1.2 MPa and $\nu = 0.44$, 0.45 and 0.46. With an experimental data of precision 2 %, it is possible to determine E within 0.1 MPa and ν within 0.1, using both G'_ω and G''_ω.

We illustrate in figure 7 the solution of the entire equation (2.11) in order to determine both the Young's modulus and the Poisson ratio of a layer in one run. We take the example of a 1 μm thick layer of Young's modulus 1 MPa and Poisson ratio 0.45 investigated with a probe of radius $R = 10\,\mu$m at a frequency 1 kHz with a viscosity $\eta = 100$ mPa s. As seen from the diagram in figure 6, this corresponds to an appropriate choice of experimental parameters for which the run-line falls on the transition between several regions. Firstly, by adjusting the force response at large distance with the master function g_n for a compressible thin film, one gets a first estimate of E'. It is then possible to plot the responses expected for a range of possible E and ν. Figure 7 shows these responses for a Young's modulus ranging from 0.8 to 1.2 MPa and a Poisson ratio from 0.44 to 0.46. As both the real and imaginary parts have to be adjusted, one sees that it is possible to determine the adequate couple (E, ν) with a precision of 10% in E and 20% in ν.

Finally, another use of the phase diagram and of the spring-and-dashpot model developed above is to estimate the amplitude of effects not included in (2.11). For instance, the effect of the substrate compliance as quantified in the previous section (4.9), defines a new line on the phase diagram parallel to the thick/thin film transition, whose position depends only on the ratio of the reduced Young's moduli of the substrate and of the layer. Below this line, one has to quantitatively take into account the substrate compliance as described in Appendix A.4. In the same light, the effect of the liquid compressibility χ can be estimated from the stiffness of a film of thickness D, $k_{liq}(D) = 2\pi R/\chi$, in series with the layer stiffness. Taking also the case of an incompressible thin film, the effect of the liquid compressibility is less than 1 % in the force response if

$$\frac{\tau}{R} > 1.8(E^*\chi)^{1/3}\left(\frac{D}{R}\right)^{2/3}. \tag{5.3}$$

If the probe radius cannot be chosen to stay above this limit, the liquid compressibility has to be taken into account as described in Appendix A.4.

6. Conclusion

In conclusion, we have shown here that forcing oscillatory flows of confined liquids provides a unique method to determine directly, quantitatively and without contact the elastic properties of supported soft layers. This method can be easily implemented on dynamic SFA or AFM in non-contact mode. It gives access to the absolute values of the Young's modulus and Poisson ratio of the surface layer, without prior knowledge of the probe/layer adhesion work, and in thin film conditions for which direct contact measurements are not quantitative.

This nanorheology method opens new perspectives for investigating the mechanical properties of thin polymer coatings and their modification under the effect of confinement and of surface interactions. More generally, it is of interest to investigate quantitatively the mechanics of fragile layers which could be altered by way of contact with a solid probe such as gas-enriched hydrophobic interfaces (Dammer & Lohse 2006; Rossky 2010), supported bubbles or soft biological layers.

This work has been partially funded by the Agence Nationale pour la Recherche program Blanc Merig.

Supplementary Material is available at journals.cambridge.org/flm.

Appendix

A.1. *Asymptotic behaviour of the force response at large distance*

At large distance, the solution of (3.1) (resp. of (4.1) and (4.4)) can be expanded in increasing powers of D_c/D as $\tilde{p}(\zeta)=\tilde{p}^{(0)}(\zeta)+\tilde{p}^{(1)}(\zeta)+\ldots$. with D_c equal to D_k (resp. D_n, $D_{1/2}$). The zero and first orders are

$$\tilde{p}^{(0)}(\zeta)=-\frac{3\mathrm{i}}{2}\zeta K_1(\zeta), \tag{A 1}$$

$$\tilde{p}^{(1)}(\zeta)=-3\mathrm{i}\left(\frac{D_c}{D}\right)^l\int_0^\infty \zeta'^m\tilde{p}^{(0)}(\zeta')\,\mathrm{d}\zeta'\int_0^\infty x\,\mathrm{d}x\frac{J_1(\zeta x)J_1(\zeta' x)}{\zeta\zeta'(1+x^2)^3}, \tag{A 2}$$

with l equal to 3/2 (resp. 2, 3) and m to 0 (resp. 1, 3) in the thick film case (resp. compressible, incompressible thin film case). This yields

$$\tilde{p}^{(1)}(0)=-\frac{9}{2}\left(\frac{D_c}{D}\right)^l\int_0^\infty \mathrm{d}\zeta' K_1(\zeta')\zeta'^m\int_0^\infty x^2\,\mathrm{d}x\frac{J_1(\zeta' x)}{2(1+x^2)^3}=-\frac{9a_{m+2}}{32}\left(\frac{D_c}{D}\right)^l, \tag{A 3}$$

$$a_{m+2}=\int_0^\infty \zeta'^{m+2}K_1^2(\zeta')\,\mathrm{d}\zeta'. \tag{A 4}$$

With $\tilde{p}^{(0)}(0)=-3\mathrm{i}/2$ and $g(D/D_c)=-(4D_c/6D)\,\tilde{p}(0)$, one gets the general expansion:

$$\lim_{D\to\infty} g\left(\frac{D}{D_c}\right)=\frac{3a_{m+2}}{16}\left(\frac{D_c}{D}\right)^{l+1}+\mathrm{i}\frac{D_c}{D}. \tag{A 5}$$

A.2. *Numerical calculation of the functions g_n, g_k, $g_{1/2}$*

We solve the integral equations (3.1), (4.1) and (4.4) by using the Numerical Recipes (Press *et al.* 1986) routines `fredin` and `fredsolve` for the Fredholm equations of type 2 together with a Gauss–Legendre quadrature (routines `gauleg` and `gaulegsub`) for calculating the integrals. The parameters used are the following: the integral on the variable ζ' is calculated on the interval (0,20) with $N=150$ points; the kernel $M(\zeta,\zeta')$

is calculated once and for all on the $N \times N$ points previously defined, and is used for solving (3.1), (4.1) and (4.4). The integral on the variable x for calculating the kernel is performed over the interval $(0, 500)$ with a Gaussian quadrature of 25 points. A table in the Supplementary Material available at journals.cambridge.org/flm, reports the numerical values of g_n, g_k, $g_{1/2}$ in the cross-over region. The relative precision is estimated better than 10^{-3}, as increasing the integration intervals and the number of points of the quadratures by 50 % does not change the result by more than this value.

A.3. *Another approach for the compressible thin film limit*

In the compressible thin film limit that we have seen in § 4.1, the elastic response of the film can be approximated as $X(y) = y(1-2\nu)/2(1-\nu)^2$. Equation (2.5) then gives the film indentation as a function of the applied pressure

$$\tilde{u}(q) = \frac{\tau}{E'}\delta\tilde{P}(q), \quad E' = \frac{E(1-\nu)}{(1-2\nu)(1+\nu)}. \tag{A 6}$$

This corresponds to a local response $u(r) = P(r)\tau/E'$ which can be directly injected in the direct space equation (2.4) to recover the same equation as Steinberger *et al.* (2008)

$$\frac{\partial}{\partial r}\left[\frac{r}{12\eta}\left(D + \frac{r^2}{2R}\right)^3 \frac{\partial \delta P(r)}{\partial r}\right] = \mathrm{i}\omega r\left(h_0 + P(r)\frac{\tau}{E'}\right). \tag{A 7}$$

A.4. *Effect of the substrate compliance and of the liquid compressibility*

The total response of the stratified system including the elastic semi-infinite substrate has been calculated by Li & Chou (1997) (see also Gacoin *et al.* 2006):

$$X(q\tau) = \frac{1 + 4bq\tau\,\mathrm{e}^{-2q\tau} - ab\mathrm{e}^{-4q\tau}}{1 - (a + b + 4b(q\tau)^2)\,\mathrm{e}^{-2q\tau} + ab\,\mathrm{e}^{-4q\tau}}, \tag{A 8}$$

$$a = \frac{\alpha\gamma_s - \gamma_l}{1 + \alpha\gamma_s}, \quad b = \frac{\alpha - 1}{\alpha + \gamma_l}, \quad \alpha = \frac{G_l}{G_s}, \qquad \gamma_s = 3 - 4\nu_s, \quad \gamma_l = 3 - 4\nu_l. \tag{A 9}$$

Here $G_i = E_i/2(1+\nu_i)$ is a shear modulus, $i = s$ refers to the substrate and $i = l$ to the layer.

When the liquid compressibility is no longer negligible, (2.11) has to be modified. One has to consider the mass conservation of the liquid in an axisymmetric geometry:

$$\frac{\partial}{\partial r}[2\pi r h(r,t) v(r,t)\rho(P(r,t))] = -\frac{\partial}{\partial t}[2\pi r h(r,t)\rho(P(r,t))], \tag{A 10}$$

taking into account the variation of the liquid density $\rho(P) = \rho_0(1 + \chi\delta P)$, with χ the liquid compressibility. The linear response for the flow is then

$$\frac{\partial}{\partial r}\left[\frac{r}{12\eta}\left(D + \frac{r^2}{2R}\right)^3 \frac{\partial \delta P(r)}{\partial r}\right] = \mathrm{i}\omega r\left[h_o + u(r) - \chi\delta P(r)\left(D + \frac{r^2}{2R}\right)\right]. \tag{A 11}$$

Integrating this equation between 0 and r, and coupling it with the elastic response of the film (2.5) in the Hankel's space yields the integro-differential equation

$$\frac{\partial \delta P(r)}{\partial r} = \frac{6\mathrm{i}\omega\eta r}{z^3} + \frac{24\mathrm{i}De}{z^3}\int_0^\infty \mathrm{d}q\,\delta\tilde{P}(q)\left[J_1(qr)\frac{X(q)}{q} + \frac{E^*\chi z}{2}J_1(qr) - \frac{E^*\chi}{2}\frac{r}{Rq}J_2(qr)\right], \tag{A 12}$$

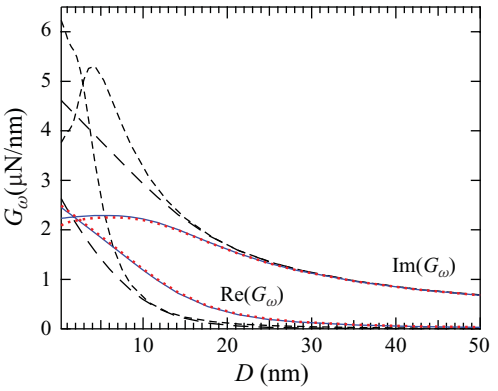

FIGURE 8. (Colour online) Illustration of the substrate compliance and of the liquid compressibility on the hydrodynamic response obtained on an incompressible 500 nm thick film of 10 MPa Young's modulus. The experiment frequency is 19 Hz, the sphere radius $R = 3$ mm, the sphere and plane Young's moduli 60 GPa and their Poisson ratio 0.2, the liquid viscosity $\eta = 0.2$ Pa.s and its compressibility $\chi = 5.10^{-10}$ Pa^{-1}. Long dashed line: the components of $G_\omega(D)$ calculated for the film with a rigid sphere and substrate. Short dashed line: components of $G_\omega(D)$ that would be obtained with the compliant sphere and substrate without film. Continuous line: the substrate and sphere compliance is taken into account using the film response given in (A 8) of Appendix A.4. Dotted line: both the sphere and substrate compliance and the liquid compressibility are taken into account using the kernel derived in (A 13) of Appendix A.4.

with $z = D + r^2/2R$. We use for this the relations: $\int_0^r s\,\mathrm{d}s J_o(qs) = r J_1(qr)/q$ and $\int_0^r s^3\,\mathrm{d}s J_o(qs) = r^3 J_1(qr)/q - 2(r^2/q^2)J_2(qr)$ derived from Abramowitz & Stegun (1964). Taking the same non-dimensional variables as in § 2 and following the same steps, one gets the new kernel to be used in (2.11)

$$M(\zeta,\zeta') = X(\zeta' t') \int_0^\infty x\,\mathrm{d}x \frac{J_1(\zeta x)J_1(\zeta' x)}{\zeta\zeta'(1+x^2)^3} + \sqrt{\frac{D}{2R}}\frac{E^*\chi}{2}\int_0^\infty \mathrm{d}x \left(\frac{x J_1(\zeta x)J_1(\zeta' x)}{\zeta(1+x^2)^2} - \frac{2x^2 J_2(\zeta' x)J_1(\zeta x)}{\zeta\zeta'(1+x^2)^3}\right). \quad \text{(A 13)}$$

Figure 8 illustrates the effect of the substrates' bulk compliance and of the liquid compressibility for a 500 nm thick incompressible film of 10 MPa modulus investigated with a sphere of radius $R = 3$ mm. For this thin film and large sphere, the substrate correction is major, and the effect of the liquid compressibility is visible only on the viscous damping at short distance.

REFERENCES

ABRAMOWITZ, M. & STEGUN, I. A. 1964 *Handbook of Mathematical Functions*. US Government Printing Office.

AIME, J. P., BOISGARD, R., NONY, L. & COUTURIER, G. 2001 Influence of noncontact dissipation in the tapping mode: attempt to extract quantitative information on the surface properties with the local force probe method. *J. Chem. Phys.* **114** (4945).

BARNOCKY, G. & DAVIS, R. H. 1988 Elastohydrodynamic collision and rebound of spheres: experimental verification. *Phys. Fluids* **31** (6), 1324.

BARNOCKY, G. & DAVIS, R. H. 1989 The influence of pressure-dependent density and viscosity of the elastohydrodynamic collision and rebound of two spheres. *J. Fluid Mech.* **209**, 501–519.

Barthel, E. 2007 Adhesive contact of a compliant sphere to an elastic coated substrate: the thin film limit. *J. Adhes.* **83**, 729.

Barthel, E. & Perriot, A. 2007 Adhesive contact to a coated elastic substrate. *J. Phys.* D*: Appl. Phys.* **40**, 1059–1067.

Barthel, E., Perriot, A., Chateauminois, A. & Frétigny, C. 2006 Elastic contact to nearly incompressible coatings – stiffness enhancement and elastic pile-up. *Phil. Mag.* **86**, 535.

Basire, C. & Fretigny, C. 1999 Determination of viscoelastic moduli at a submicrometric scale. *Eur. Phys. J. Appl. Phys.* **6**, 323–329.

Bodiguel, H. & Fretigny, C. 2006 Reduced viscosity in thin polymer films. *Phys. Rev. Lett.* **97**, 266105.

Chan, D. C. Y. & Horn, R. G. 1985 The drainage of thin films between solid surfaces. *J. Chem. Phys.* **83**, 5311.

Cottin-Bizonne, C., Steinberger, A., Cross, B., Raccurt, O. & Charlaix, E. 2008 Nanohydrodynamics: the intrinsic boundary flow condition on smooth surfaces. *Langmuir* **24**, 1165–1172.

Dammer, S. M. & Lohse, D. 2006 Gas enrichment at liquid–wall interfaces. *Phys. Rev. Lett.* **96**, 206101.

Davis, R. H., Serayssol, J.-M. & Hinch, E. J. 1986 The elastohydrodynamic collision of two spheres. *J. Fluid Mech.* **163**, 479–497.

Dubourg, F., Aime, J. P., Marsaudon, S., Couturier, G. & Boisgard, R. 2003 Probing the relationship between the scales of space and time in an entangled polymer network with an oscillating nanotip. *J. Phys. Condens. Matter* **15** (36), 6167–6177.

Ducker, W. A. 2009 Contact angle and stability of interfacial nanobubbles. *Langmuir* **25** (16), 8907–8910.

Gacoin, E., Fretigny, C., Chateauminois, A., Perriot, A. & Barthel, E. 2006 Measurement of the mechanical properties of thin films mechanically confined within contacts. *Tribol. Lett.* **21** (3), 245–252.

Georges, J.-M., Milliot, S., Loubet, J. L. & Tonck, A. 1993 Drainage of thin liquid films between relatively smooth surfaces. *J. Chem. Phys.* **98**, 7345.

Hocking, L. M. 1973 The effect of slip on the motion of a sphere close to a wall and of two adjacent spheres. *J. Engng Maths* **7**, 207.

Honig, C. D. F. & Ducker, W. A. 2007 No-slip hydrodynamic boundary condition for hydrophilic particles. *Phys. Rev. Lett.* **98** (2), 028305.

Huang, D. M., Sendner, C., Horinek, D., Netz, R. R. & Bocquet, L. 2008 Water slippage versus contact angle: a quasi-universal relationship. *Phys. Rev. Lett.* **101**, 226101.

Johannsmann 2002 The glass transition and contact mechanical experiments on polymer surfaces. *Eur. Phys. J.* E **8**, 257–259.

Johnson, K. L., Kendall, K. & Roberts, A. D. 1971 Surface energy and the contact of elastic solids. *Proc. R. Soc. Lond.* A **324**, 301–313.

Lauga, E. & Brenner, M. P. 2004 Dynamic mechanisms for apparent slip on hydrophobic surfaces. *Phys. Rev.* E **70**, 026311.

Leopoldes, J. & Jia, X. 2009 Probing viscoelastic properties of a thin polymer film sheared between a beads layer and an ultrasonic resonator. *Eur. Phys. Lett.* **88**, 34001.

Li, J. & Chou, T.-W. 1997 Elastic field of a thin-film/substrate system under an axisymmetric loading. *Intl J. Solids Struct.* **34** (35–36), 4463–4478.

Long, D. & Lequeux, F. 2001 Heterogeneous dynamics at the glass transition in van der Waals liquids, in the bulk and in thin films. *Eur. Phys. J.* E **4**, 371–387.

Mary, P., Chateauminois, A. & Fretigny, C. 2006 Deformation of elastic coatings in adhesive contacts with spherical probes. *J. Phys.* D*: Appl. Phys.* **39**, 3665–3673.

McGuiggan 2004 Measurement of the loss tangent of a thin polymeric film using the atomic force microscope. *J. Mater. Res.* **19** (1), 387–395.

McGuiggan, P. M., Wallace, J. T., Smith, D. T., Sridhar, I., Zheng, Z. W. & Johnson, K. L. 2007 Contact mechanics of layered elastic materials: experiment and theory. *J. Phys.* D*: Appl. Phys.* **40**, 5984–5994.

Nogi, T. & Kato, T. 1997 Influence of a hard surface layer on the limit of elastic contact. – Part 1. Analysis using a real surface model. *ASME J. Tribol.* **119** (3), 493–500.

O'Connell, P. A. & McKenna, G. B. 2005 Rheological measurements of the thermoviscoelastic response of ultrathin polymer films. *Science* **307**, 5716.

Perriot, A. & Barthel, E. 2004 Contact to a coated half-space: effective elastic modulus and real penetration. *J. Mater. Res.* **19**, 600.

Press, W. H., Flannery, B. P., Teukolsky, S. A. & Vetterling, W. T. 1986 *Numerical Recipes: The Art of Scientific Computing*. Cambridge University Press.

Raviv, U., Perkin, S., Laurat, P. & Klein, J. 2004 Fluidity of water confined to subnanometer films. *Langmuir* **20**, 5322–5332.

Restagno, F., Crassous, J., Charlaix, E., Cottin-Bizonne, C. & Monchanin, M. 2002 A highly sensitive dynamic surface force apparatus for nanorheology. *Rev. Sci. Instrum.* **73**, 2292–2297.

Rossky, P. J. 2010 Exploring nanoscale hydrophobic hydration. *Faraday Discuss.* **146**, 13–18.

Shull, K. R. 2002 Contact mechanics and the adhesion of soft solids. *Math. Sci. Engng Res.* **36** (1), 1–45.

Sridhar, I. & Johnson, K. L. 2004 A detailed analysis of adhesion mechanics between a compliant elastic coating and a spherical probe. *J. Phys.* D*: Appl. Phys.* **37**, 2886–2895.

Stafford, C. M., Harrison, C., Beers, K. L., Karim, A., Amis, E. J., Vanlandingham, M. R., Kim, H.-C., Volksen, W., Miller, R. D. & Simonyi, E. E. 2004 A buckling-based metrology for measuring the elastic moduli of polymeric thin films. *Nature Mater.* **3**, 545.

Steinberger, A., Cottin-Bizonne, C., Kleimann, P. & Charlaix, E. 2008 Nanoscale flow on a bubble mattress: effect of surface elasticity. *Phys. Rev. Lett.* **100**, 134501.

Tardivat, C., Hervet, H. & Leger, L. 2001 Adhesion evaluation for a stratified system in JKR geometry. *J. Adhes. Sci. Technol.* **15** (9), 1055–1078.

Vinogradova, O. I. & Feuillebois, F. 2000 Elastohydrodynamic collision of two spheres allowing slip on their surfaces. *J. Colloid Interface Sci.* **221**, 1–21.

Yang, S., Dammer, S. M., Bremond, N., Zandvliet, H. J. W., Kooij, E. S. & Lohse, D. 2007 Characterization of nanobubbles on hydrophobic surfaces in water. *Langmuir* **23**, 7072–7077.